Acid SAPO-34 Catalysts for Oxidative Dehydrogenation of Ethane

L. Marchese,*,1 A. Frache,* G. Gatti,* S. Coluccia,† L. Lisi,‡ G. Ruoppolo,§ G. Russo,‡ and H. O. Pastore¶

*Dipartimento di Scienze e Tecnologie Avanzate, Università del Piemonte Orientale "A. Avogadro," C. so Borsalino 54, I-15100 Alessandria, Italy;
†Dipartimento di Chimica IFM, Università di Torino, v. P. Giuria 7, I-10125 Torino, Italy; ‡Istituto di Ricerche sulla Combustione, CNR, P. le
Tecchio 80, 80125 Naples, Italy; §Dipartimento di Ingegneria Chimica, Università di Napoli "Federico II," P. le Tecchio 80, 80125 Naples,
Italy; and ¶Instituto de Química, Universidade Estadual de Campinas, CP 6154, CEP 13083-970, Campinas, SP, Brasil

Acid SAPO-34-based microporous catalysts with chabasite structure have been tested for the oxidative dehydrogenation of ethane in the temperature range 550–700°C. Pure acid and La/Na-containing samples were monitored and very interesting catalytic performances were achieved at 550–700°C (75–60% C_2H_4 selectivity and 5–30% ethane conversion) with respect to those reported for both acid zeolites and metal oxides. These performances correlated to the Brønsted acidity probed by FTIR spectroscopy and temperature-programmed desorption of NH_3. The number of Brønsted acid sites located at the bridging hydroxyls (3626–3600 cm^{-1}) in acidic SAPO-34 was higher than in La- and Na-containing samples, which showed also a larger amount of P–OH at framework defects. Lewis acidity induced by the presence of La and Na ions also influenced the reactivity of the SAPO-34-based catalysts. © 2002 Elsevier Science (USA)

Key Words: SAPO-34; LaAPSO-34; oxidative dehydrogenation; ethane; Lewis and Brønsted acidity.

INTRODUCTION

The oxidative dehydrogenation (ODH) of light alkanes would be a promising alternative to industrial processes for the production of olefins provided these very reactive products are not further oxidized during the process (1). As far as the ethane ODH reaction is concerned, transition metal oxides, basic oxides such as Li/MgO, and rare earth oxides have been extensively studied (2–8). The reaction occurs through a redox cycle on the surface of transition metal oxide catalysts whereas a promotion of ethyl radicals is the key step of those based on Li/MgO or on rare earth oxides which show a better selectivity (7). However, transition metal oxides, although quite active at lower temperatures, give very poor selectivity to ethylene at high ethane conversions (low ethylene yields) because of the oxidation of the adsorbed intermediates by lattice oxygens. In the case of Li/MgO, good selectivity was achieved at higher ethane conversions due to the rapid desorption of the ethyl intermediate which reacts

with O_2 in the gas phase, resulting in a significant enhancement of ethylene yields (7, 8). The C_2H_4 selectivity limit value (about 60%) determined by the above-mentioned homogeneous reaction has been overcome by adding Na to a lanthanum oxide-based catalyst (La_2O_3–$NaAlO_2$). The catalytic properties of this new system were thus modified and, through the promotion of a surface reaction, led to higher ethylene selectivity at good ethane conversions with a further increase in the olefin yield (7).

Therefore, the increase in the selectivity to alkenes at significant alkane conversion is highly desirable and, in principle, may be emphasized if the reaction is conducted within the restricted space of zeolitic cages or channels. Zeolite-based catalysts have been tested for oxidative dehydrogenation of light alkanes (8–11), but either the role of the structure or the presence of acid sites in activating the reaction has not yet been fully understood. It is reported, for instance, that strong Brønsted acid sites are undesired for ethane ODH reaction, whereas the presence of transition metal cations enhanced both activity and selectivity (10). In other zeolite-type aluminophosphates catalysts with AEL and AFI structures containing Fe, Cr, Mn, and V, low alkene selectivity at high alkane conversion has been achieved (12, 13). Likewise, the introduction of V, Co, Mg, or Mn into a medium-pore ALPO-5 structure provided good activity at 425–600°C, but ethylene selectivity did not exceed 65% at 7.5% ethane conversion (14, 15).

Small-pore zeolites, however, may play a decisive role for enhancing the selectivity to light alkenes precisely due to the constrained environments where the reactions are to take place. In this direction we have tested SAPO-34 for ethane ODH reaction. SAPO-34 is an acid silico-aluminophosphate with chabasite-related structure (16) where the access to the micropores is limited by eight-membered rings (3.8 Å). This zeo-type material has Brønsted acid sites which catalyze the methanol-to-olefin (MTO) reaction very selectively to C_2–C_3 products (17–19).

This work shows that SAPO-34 is also a good catalyst for ethane ODH reaction, the high thermal stability of the chabasite structure [20] being fundamental when the reaction is activated at temperatures of 600–700°C. The

catalytic performances of SAPO-34 materials containing Na and La ions, and their acid properties, have been also monitored in the present study and compared with those of a nonporous La_2O_3–$NaAlO_2$ mixed-phase catalyst with very good ethylene yields (7).

EXPERIMENTAL

SAPO-34 was synthesized by mixing appropriate amounts of $Al(OH)_3$ (Aldrich), orthophosphoric acid (85%, Aldrich), and distilled water. The mixture was stirred up to the point of obtaining a uniform gel. SiO_2 (Aerosil 200, Degussa) and morpholine, the structural directing agent, were added to obtain gels with the composition reported in Table 1. To prepare Na- and La-containing samples (NaAPSO-34 and LaAPSO-34) NaOH and $La(NO_3)_3$ were mixed before adding the organic template. After a vigorous stirring, the resulting gel was crystallized in stainless steel, teflon-lined, autoclaves under autogeneous pressure at 195°C for 10 days, and the product was filtered, washed with water, and dried in air at room temperature.

The crystalline product was characterized by XRD using a Shimadzu XRD6000 with Cu$K\alpha$, at 2° 2θ min^{-1}, with slits of 1°, 1°, and 0.3 mm for scattering, divergence, and receiving. High-temperature experiments were conducted with the aid of a Shimadzu heating accessory model HA1001, at a heating rate of 5°C/min. BET surface area measurements (Carlo Erba 1900 Sorptomatic) and scanning electron micrographs (SEM, Leica Stereoscan 420 equipped with EDS attachment) were performed for the available area and morphology of the material. No extra phases were detected either by XRD or by SEM. FTIR spectra (resolution of 4 cm^{-1}) were collected on pelletized samples using an ATI Mattson Spectrometer equipped with a high-vacuum, variable-temperature infrared cell (LB-100 by Infraspac Ltd, Novosibirsk, Russia). TGA (TA instrument, SDT2960) analyses were run under vacuum or gas flow (He or air). Changes in the heating rate were evaluated for optimizing the conditions to remove the morpholine and activate the material before the catalytic tests. The following procedure was found to give catalysts with high crystallinity and surface areas: (a) heating under helium flow at 5°C/min up to 600°C and leaving at this temperature for 20–30 h; (b) switching the gas to oxygen flow and leaving for 10–15 h. Temperature programmed desorption (TPD) of NH_3 was carried out on the activated catalysts using a Micromeritics TPD/TPR 2900 analyser equipped with a TC detector and coupled with a Hiden HPR 20 mass spectrometer. The activated samples were saturated with pure ammonia at 100°C for 1 h and, after purging with pure He for 2 h, heated at 10°C min^{-1} to 700°C under helium flow (25 cm^3 min^{-1}).

The catalytic activity tests were carried out with a fixed-bed quartz microreactor operating under atmospheric pressure, at temperatures ranging from 550 to 700°C and contact times from 0.03 to 0.17 g·s·N·cm^{-3}. The feed compositions were 4% C_2H_6 and 1–5% O_2 in a balance of He. In order to limit the homogeneous contribution to ethane conversion, the catalytic bed was filled up with α-Al_2O_3 pellets and the reactor diameter was reduced in the postcatalytic zone. The contribution of homogeneous reactions and/or of the α-Al_2O_3 was verified by performing blank runs up to 700°C under the same reaction conditions of catalytic tests and with the reactor containing only α-Al_2O_3. No significant ethane conversions were obtained in the blank experiment.

RESULTS AND DISCUSSION

Figure 1A shows the SEM micrograph of an as-synthesized LaAPSO-34 sample where the rhombohedral shape of the microcrystals, which is typical of these systems (21), is clearly observed. Crystals with average dimensions of about 10 μm can be obtained using this synthesis procedure. The EDS signal for the lanthanum ions (Fig. 1B) at 4.651 KeV was observed and found to be nearly homogeneously distributed practically in all crystals. Both SAPO-34 and NaAPSO-34 samples showed a similar rhombohedral shape of the crystals, though with slightly different particle size distribution.

Figure 2 shows X-ray diffractograms for a SAPO-34 sample collected *in situ* at increasing temperatures, under air, and clearly suggests that the chabasite structure is not affected significantly up to 900°C. Only at 1000°C is the incipient formation of a tridimite dense phase (reflection at 21° 2θ) detected, but even at this temperature the zeolitic phase is present in an appreciable amount. Na- and La-containing SAPO-34 samples, as well as the ALPO-34 one, showed very similar results, and this suggests that the presence of Na and La ions does not affect the stability of the chabasite structure.

FTIR spectroscopy was used for monitoring the presence of hydroxyls in all the materials used. Two types of bridging hydroxyls [Si-O(H)-Al] absorbing at 3625 and 3600 cm^{-1} were found in the case of the SAPO-34 catalyst (Fig. 3a), and these are the active sites for acid-catalyzed reactions (16–18). P–OH and Si–OH absorbing respectively at 3675

TABLE 1

Composition (Molar Ratios) of the Gels Used to Synthesize the Materials Studied in This Work

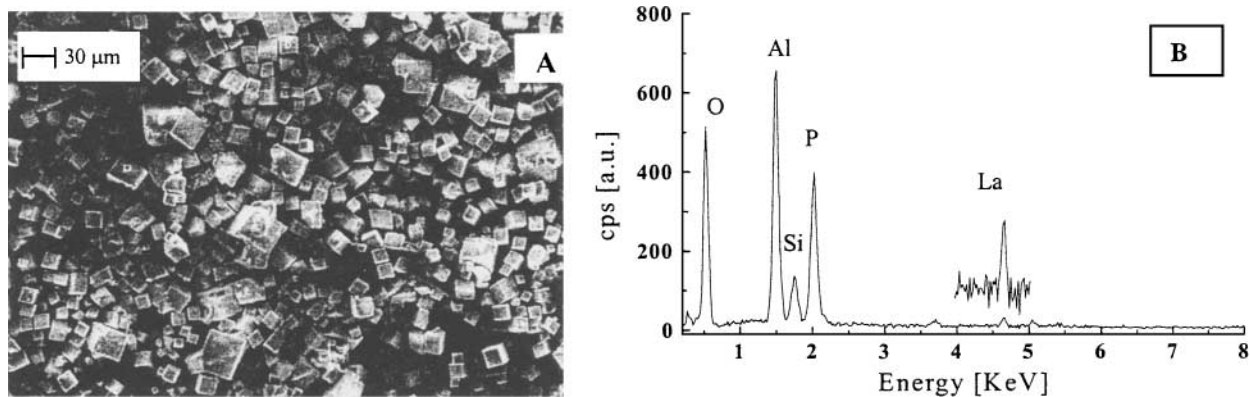| Sample	Metal ion (Na or La)	Si	Al	P	HF	Morpholine	H_2O
AlPO-34	—	—	1.0	1.0	0.35	1.25	50
SAPO-34	—	0.3	1.0	0.90	—	1.25	50
NaAPSO-34	0.15	0.3	1.0	0.90	—	1.25	50
LaAPSO-34	0.04	0.2	1.0	0.90	—	1.25	50

FIG. 1. Scanning electron micrograph of as-synthesized LaAPSO-34 (A) and an EDS spectrum of a LaAPSO-34 microcrystal (B).

and 3743 cm^{-1} were also detected. These hydroxyls are located at defects (internal or external surface) sites of the crystals and might be also involved in ODH reactions run at high temperatures.

Although in different concentrations, all these hydroxyls were present in both LaAPSO-34 (Fig. 3b) and NaAPSO-34 (Fig. 3c). In particular, bridging hydroxyls were less abundant in La- and Na-containing materials and their amount depended on the loading of the cations inserted during the synthesis. Only semiquantitative data can be obtained by these IR measurements; however, they clearly suggest that a part of the negative charges of the framework, produced by Si insertion at P sites, was balanced by lanthanum and sodium cations. Moreover, when these cations were present, a larger number of P–OH groups were found at defect sites of the chabasite structure, and this was particularly evident in the case of La-containing material. The AlPO-34 sample (Fig. 3d) showed a very small number of POH groups; in fact only an extremely weak band at 3675 cm^{-1} was found. It is noteworthy that this figure correlated with the NH$_3$-TPD results (*vide infra*).

The active catalysts were prepared from the as-synthesized material by calcining the structure-directing
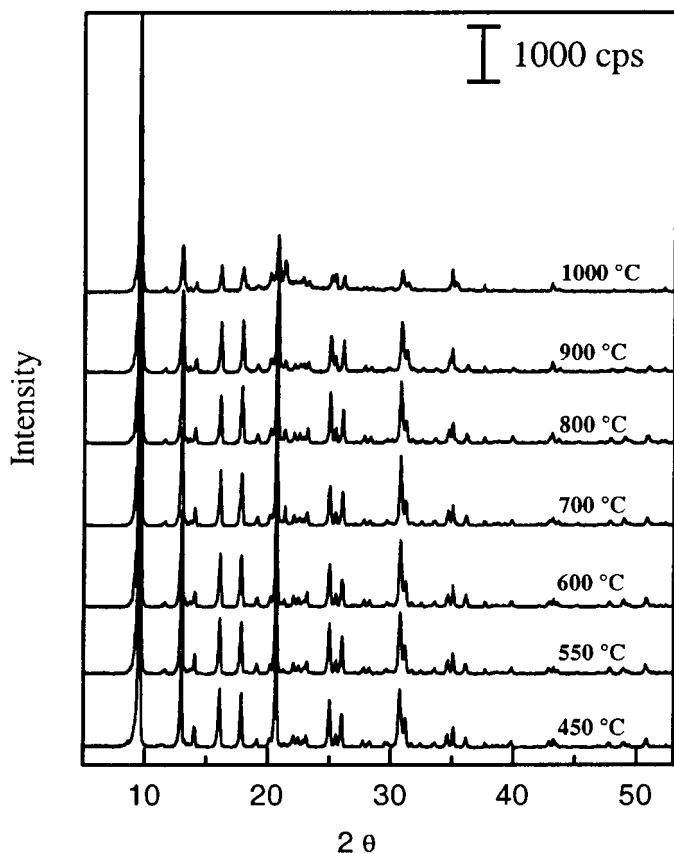

FIG. 2. XRD patterns of SAPO-34 upon thermal treatments of 450–1000°C in the XRD heating chamber.
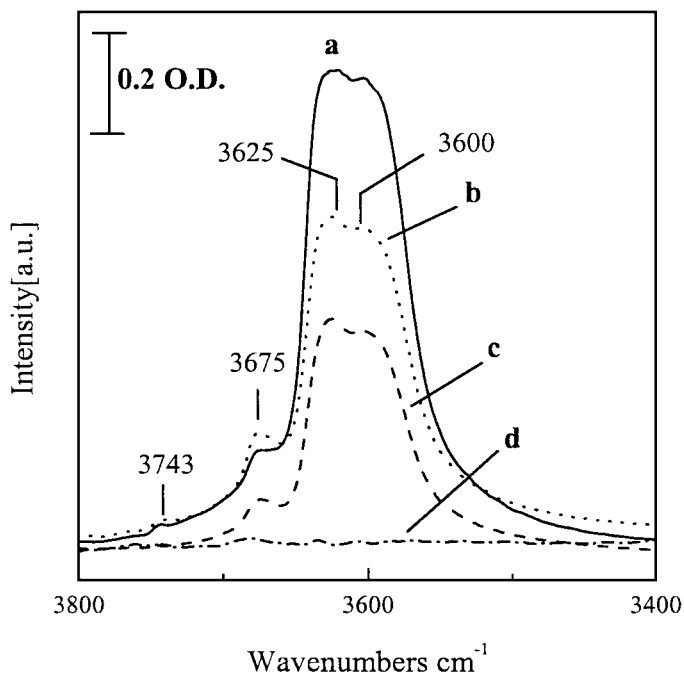

FIG. 3. FTIR spectra of SAPO-34 (a), LaAPSO-34 (b), NaAPSO-34 (c), and AlPO-34 (d).

agent, normally at around 550–600°C. As the catalytic reaction was studied at temperatures up to 700°C, it was necessary to check for the presence of hydroxyls by FTIR and for structure stability by XRD under these temperature conditions. The structure is preserved at the running temperature, and FTIR spectra recorded before and after heating at 700°C (spectra not shown for sake of brevity) showed that the number of Brønsted acid sites did not vary significantly at temperatures ranging from 550 to 700°C.

TGA experiments under vacuum, in He, and in oxygen flow were performed to define a reproducible calcination procedure. The weight loss due to morpholine decomposition or combustion started at around 350°C and was complete at 600–650°C, giving H_2O, CO_2, and N_2O under oxidative conditions (air flow), whereas H_2, H_2O, CO, CO_2, amine, ethylene, and heavier fragments were formed under decomposition conditions (vacuum or helium flow). A combined FTIR and gas chromatography–mass spectrometry study showed that the formation of H_2 and ethylene during the morpholine decomposition was more pronounced on samples with a larger number of Brønsted acid sites and this is evidence of the fact that the dehydrogenating properties of SAPO-34 catalysts are related to their acid properties.

In order to avoid hot spots and structure damage, prolonged thermal treatments in He (20–30 h) were needed to guarantee that a higher fraction of morpholine was decomposed before calcining the organic products under oxygen. Samples with BET surface areas of 220–340 $m^2 \cdot g^{-1}$ (Table 2) were obtained after these thermal treatments.

NH_3-TPD profiles showed two desorption steps, occurring at 250–300 and 500–600°C (Fig. 4), attributed to Lewis acid sites and/or P–OH groups (or other zeolitic defects) and bridged hydroxyls [Si–O(H)–Al], respectively (23). As is expected, the second signal was absent for the ALPO-34 sample on which only a very small number of POH groups were found. In this case Lewis acid sites at framework defects (24) might be responsible for the NH_3-TPD peak. Results of the overall integration of the NH_3-TPD curves and those of the contribution of the two mentioned peaks, obtained by a fitting procedure, are reported in Table 2. The introduction of sodium cations (Na/Si = 0.5) led to the neutralization of a significant number of Brønsted acid sites (Table 2), mostly of Si–O(H)–Al type, whereas the introduction of a very small amount of a rare earth cation
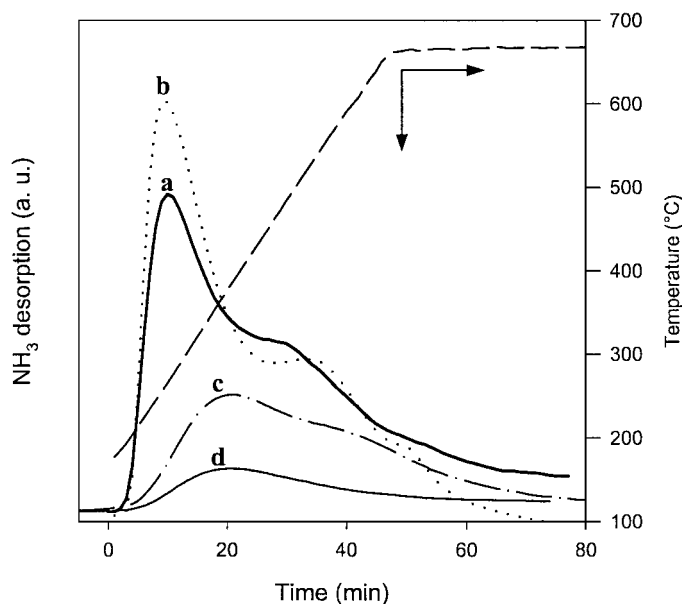

FIG. 4. TPD profiles of SAPO-34 (a), LaAPSO-34 (b), NaAPSO-34 (c), and AlPO-34 (d) catalysts.

(La/Si = 0.13) increased the number of low-temperature acid sites, likely because of the increase in P-OH groups (see IR results), as well as in Lewis acid centers.

Ethylene, CO, and CO_2 were detected as products in the catalytic tests. Traces of methane were formed only at higher conversions, and this makes SAPO-34-based catalysts quite distinct from other zeolites. In addition to ethylene and CO_x products, in fact, CH_4 and higher hydrocarbons (C_{3+}) were found on HZSM-5-based catalysts consequent to the presence of cracking reactions (9, 10). These undesired reactions led also to the formation of carbonaceous materials responsible for the catalyst deactivation. It is of great significance that cracking reactions are strongly inhibited on SAPO-34 catalysts where *deactivation effects were practically absent even after a 12-h experiment.*

Figure 5 shows the effect of contact time and O_2 partial pressure in the inlet gas mixture on both ethane conversion and products selectivity for a SAPO-34 catalyst. Good catalytic performances were obtained at 700°C (60–55% C_2H_4 selectivity and 5–30% ethane conversion at 0.12 $g \cdot s \cdot N \cdot cm^{-3}$ contact time; 75–60% C_2H_4 selectivity and 7–20% ethane conversion at 2 vol% O_2) showing that the absence of easily reducible metal ions avoids the rapid decrease of C_2H_4 selectivity at higher C_2H_6 conversions found for metal-containing ALPO-5 catalysts (14, 15). In fact, the introduction of V, Co, Mg, or Mn into the ALPO-5 structure provided good activity at 425–600°C, but the ethylene selectivity did not exceed 65% at 7.5% ethane conversion, and the value of contact time used was one order of magnitude greater than that used for the SAPO-34-based catalysts studied in the present work.

The decrease of ethylene selectivity was balanced by the formation of CO_x side products, suggesting that ethylene

TABLE 2

NH_3-TPD and BET Surface Area Results

Catalyst	Surface area ($m^2 \cdot g^{-1}$)	NH_3 desorb. low temp. ($mmol \cdot g^{-1}$)	NH_3 desorb. high temp. ($mmol \cdot g^{-1}$)	NH_3 desorb. total ($mmol \cdot g^{-1}$)
AlPO-34	377	0.43	—	0.43
SAPO-34	339	0.98	0.72	1.70
NaAPSO-34	283	0.73	0.39	1.12
LaAPSO-34	224	1.35	0.63	1.98

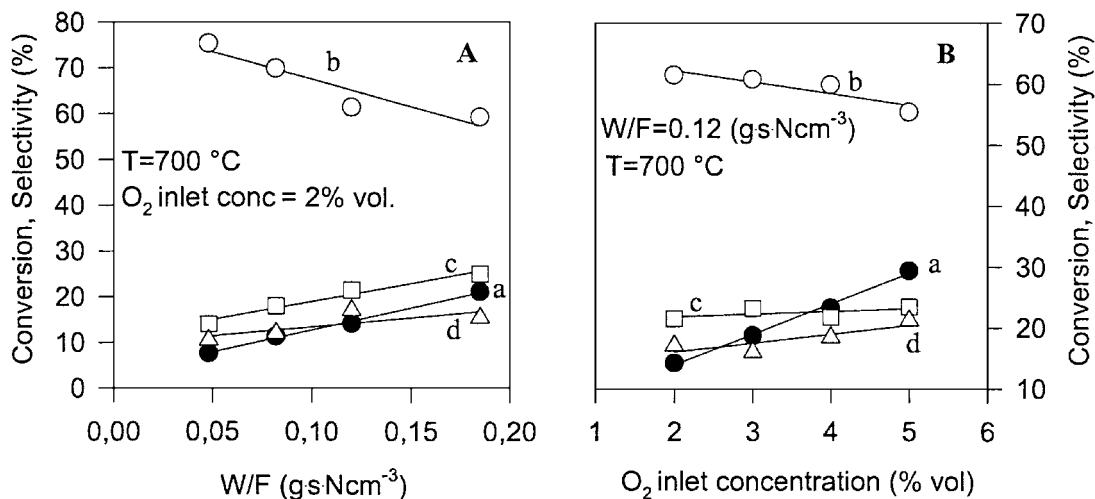**FIG. 5.** Ethane conversion (a—●) and ethylene (b—○), CO (c—□), and CO_2 (d—△) selectivity as a function of contact time (W/F) (A) and O_2 inlet concentration (B) for SAPO-34 catalyst.

oxidation could occur especially at higher contact times or higher O_2 partial pressures. The reaction temperature did not have a significant influence on the product distribution, suggesting that no changes in the reaction mechanism occurred in the interval of temperature explored. Figure 6 shows the case of LaAPSO-34, which provided the highest catalytic performances, leading to 77–70% ethylene selectivity at 5–25% conversions in the 550–700°C temperature range.

In order to clarify whether the Brønsted acid sites are involved in the ethane ODH reaction, reaction rates of ethane consumption and ethylene formation, estimated under differential reactor conditions, were reported as a func-

tion of the number of acid sites, evaluated from the high-temperature peaks in the NH_3-TPD experiments (Fig. 7). The good correlation obtained suggests that bridging hydroxyls groups are involved in ethane activation. However, a very good correlation was also obtained for the total number of acid centers and this means that the reaction should take place on both Lewis and Brønsted sites. This result concerning the ability of Lewis acid sites to activate the ODH reaction of light alkanes is in agreement with that found for zeolite-based catalysts (8–11). A more detailed spectroscopic characterization with the aid of molecular probes must be run in order to clarify the respective roles of Lewis
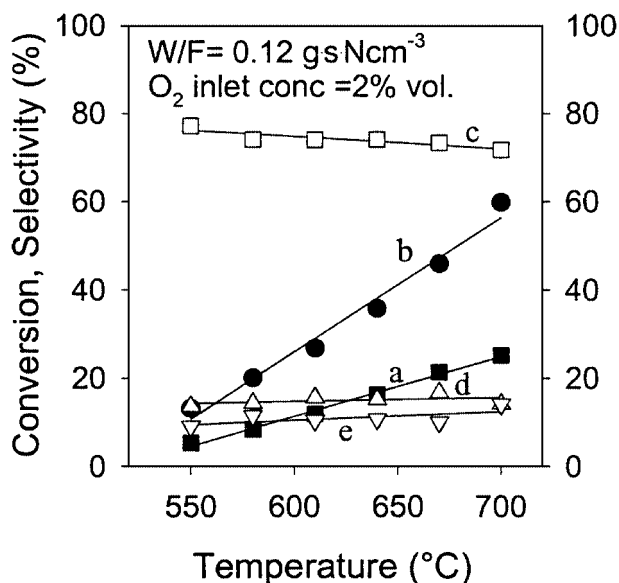

FIG. 6. Ethane (a—■) and oxygen (b—●) conversion and ethylene (c—□), CO (d—△), and CO_2 (e—▽) selectivity as a function of temperature for LaAPSO-34 catalysts.
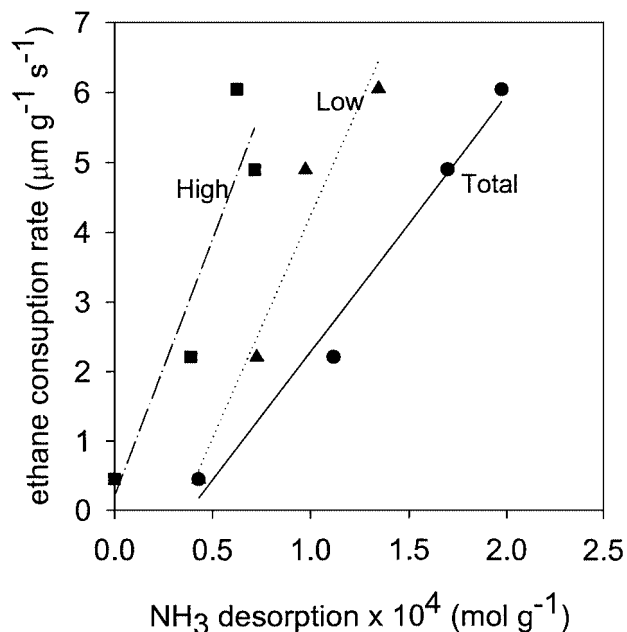

FIG. 7. Rate of ethane consumption and ethylene formation as a function of the amount of NH_3 desorbed under low- and high-temperature conditions as evaluated from TPD experiments.
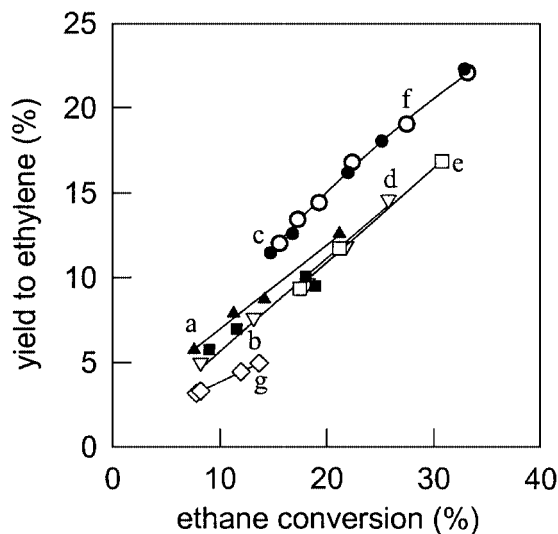
FIG. 8. Comparison between ethylene yields obtained with SAPO-34 (a—▲), Na-APSO (b—■), La-APSO (c—●), and rare earth oxide-based catalysts Sm_2O_3 (d—▽), 5% La_2O_3/MgO (e—□), and 90% La_2O_3-NaAlO$_2$ (f—○) at 700°C, as reported in (7), and 6 wt% V_2O_5/TiO$_2$ (g—◇) at 550°C, as reported in (20), as a function of ethane conversion.

and Brønsted acid sites in ODH reactions. This is, however, beyond the scope of the present article. The main purpose of this work, in fact, is to show that small-pore SAPO-34-based catalysts are active in ODH reactions and lead to superior performances with respect to medium-pore zeolites and AlPOs.

The catalytic performances of acid SAPO-34-based materials were compared (Fig. 8), under similar reaction conditions, to that of rare earth oxide-based catalysts, which provided interesting ethylene yields, especially when containing Na ions (7), through a hetero-homogeneous mechanism controlled by gas-phase reaction between ethyl radicals and O_2. In the case of SAPO-34, yields very close to those reported for rare earth oxide-based catalysts were obtained at 10–20% ethane conversions and O_2 conversions lower than 100%. These values were slightly reduced for the Na-containing catalyst whereas the introduction of La ions resulted in increasing C_2H_4 yields, which become similar to those of La_2O_3–NaAlO$_2$ catalyst. Otherwise, supported vanadium oxide catalysts, although very active at low temperature (550°C), provide very poor ethylene yields especially at high ethane conversions (22), as suggested by the lower slope of the yield/conversion curve. It is worth noting that for all SAPO-34-based catalysts these yields have been obtained with selectivity to ethylene far exceeding the limit value of about 60% reported for samarium and lanthanum oxides, determined by the homogeneous reaction between the ethyl radical and O_2 (7). This suggests that the reaction occurred within the chabasite cages and enlightens the potential of the SAPO-34 acid catalysts for ethane ODH.

In conclusion, this contribution shows that SAPO-34-based catalysts are very selective to ethylene in the ox-

idative dehydrogenation of ethane in that both ethylene oxidation to carbon oxides and cracking reactions are significantly inhibited by the zeolite structure and/or the acid character of the catalysts. The introduction of variable amounts of alkaline and alkaline earth metal ions in the SAPO-34 structure might allow modulation of the acid properties (number and strength of acid sites) of the catalysts, as well as in the accessibility to ethane, giving more hints on the role of Lewis and Brønsted acidity in zeolite-type catalysts in activating ethane ODH reaction. Work in this direction is in progress.

REFERENCES

1. Cavani, F., and Trifirò, F., *Catal. Today* **24**, 307 (1995).
2. Conway, S. J., Wang, D. J., and Lunsford, J. H., *Appl. Catal. A* **79**, L1 (1991).
3. Baerns, M., and Buyevskaya, O., *Catal. Today* **45**, 13 (1998).
4. Kennedy, E. M., and Cant, N. W., *Appl. Catal. A* **87**, 171 (1992).
5. Chourdary, V. R., and Rane, V. H., *J. Catal.* **135**, 310 (1992).
6. Bordoni, S., Castellani, F., Cavani, F., Trifirò, F., and Kulkarni, M. P., *in* "New Developments in Selective oxidation II" (V. Cortés Corberan and S. Vic Bellon, Eds.), p. 93. Elsevier, Amsterdam, 1994.
7. Ciambelli, P., Lisi, L., Pirone, R., Ruoppolo, G., and Russo, G., *Catal. Today* **61**, 317 (2000).
8. Banãres, M. A., *Catal. Today* **51**, 319 (1999).
9. Chang, Y.-F., Somorjai, G., and Heinemann, H., *Appl. Catal. A* **96**, 305 (1993).
10. Chang, Y.-F., Somorjai, G., and Heinemann, H., *J. Catal.* **154**, 24 (1995).
11. Kubacka, A., Wloch, E., Sulikowski, B., Valenzuela, R. X., and Cortés Corberan, V., *Catal. Today* **61**, 343 (2000).
12. Arends, I. W. C. E., Sheldon, R. A., Wallau, M., and Schuchardt, U., *Angew. Chem. Int. Ed. Engl.* **36**, 1144 (1997).
13. Huff, M., and Schmidt, L. D., *J. Phys. Chem.* **97**, 11815 (1993).
14. Wan, B. Z., and Huang, K. T., *Appl. Catal.* **73**, 113 (1991).
15. Concepcion, P., Corma, A., Lopes Nieto, J. M., and Perez-Pariente, J., *Appl. Catal. A* **143**, 17 (1996).
16. Smith, L., Marchese, L., Cheetham, A. K., Thomas, J. M., Wright, P. A., Chen, J., and Morris, R. E., *Science* **271**, 799 (1996).
17. Smith, L., Cheetham, A. K., Marchese, L., Gianotti, E., Thomas, J. M., Wright, P. A., and Chen, J., *Catal. Lett.* **41**, 13 (1996).
18. Chen, J., Wright, P. A., Thomas, J. M., Natarajan, S., Marchese, L., Bradley, S. M., Sankar, G., Catlow, C. R. A., Gai-Boyes, P. L., Townsend, R. P., and C. M. Lok, *J. Phys. Chem.* **98**, 10216 (1994).
19. Stöcher, M., *Microporous Mesoporous Mater.* **29**, 348 (1999).
20. Briend, M., Vomscheid, R., Peltre, M. J., Man, P. P., and Barthomeuf, D., *J. Phys. Chem.* **99**, 8270 (1995).
21. Marchese, L., Frache, A., Gianotti, E., Martra, G., Causà, M., and Coluccia, S., *Microporous Mesoporous Mater.* **145**, 30 (1999).
22. Viparelli, P., Ciambelli, P., Lisi, L., Ruoppolo, G., Russo, G., and Volta, J. C., *Appl. Catal. A* **184**, 291 (1999).
23. Popova, M., Minchev, Ch., and Knazirev, V., *Appl. Catal. A* **169**, 227 (1998).
24. Marchese, L., Chen, J., Thomas, J. M., Coluccia, S., and Zecchina, A., *J. Phys. Chem.* **98**, 13350 (1994).